

Instability of skyrmions in magnetic fields

Loïc Mougel,¹ Patrick M. Buhl,² Ryohei Nemoto,³ Timofey Balashov,¹ Marie Hervé,^{1,4} Julian Skolaut,¹ Toyo Kazu Yamada,^{3,5} Bertrand Dupé,^{6,7} and Wulf Wulfhekel¹

¹*Physikalisches Institut, Karlsruhe Institute of Technology, 76131 Karlsruhe, Germany*

²*Institute of Physics, Johannes Gutenberg University Mainz, 55099 Mainz, Germany*

³*Department of Materials Science, Chiba University, 1-33 Yayoi-cho, Inage-ku, Chiba 263-8522, Japan*

⁴*Institut des Nanosciences de Paris, Sorbonne University, CNRS-UMR7588, 75005 Paris, France*

⁵*Molecular Chirality Research Centre, Chiba University, 1-33 Yayoi-cho, Inage-ku, Chiba 263-8522, Japan*

⁶*Fonds de la Recherche Scientifique (FNRS), B-1000 Bruxelles, Belgium*

⁷*Nanomaterials/CESAM, Université de Liège, B-4000 Sart Tilman, Belgium*

(Dated: June 16, 2020)

In this combined experimental and theoretical work, we report on the evolution of the skyrmion radius and their destruction in the system Co/Ru(0001), when an out-of-plane magnetic field is applied. At low fields, skyrmions are metastable and display an elliptical instability in which along the short axis, the spin texture approaches that of the spin-spiral phase and the long axis expands in order to go back to the spin-spiral ground state. At high fields, we observe round skyrmions of finite size up to the collapse field B_c , where they are destroyed and the topological charge is annihilated. We estimate B_c via numerical methods based on magnetization dynamics simulations parametrized by density functional theory (DFT) calculations and compare it to experimental scanning tunneling microscopy (STM) observations obtained at ≈ 30 mK.

Magnetic skyrmions are localized topologically protected structures, in which the magnetization field winds around a magnetization core, such that no continuous transformation allows the conversion into a topologically trivial, homogeneously magnetized ferromagnetic (FM) state^{1–3}. The energetic stability of the skyrmions originates from the unique sense of rotation of the magnetization due to the chiral Dzyaloshinskii-Moriya interaction (DMI) which occurs when structural inversion symmetry is broken and spin-orbit coupling is present⁴. Due to this protection, skyrmions are considered as magnetic quasi-particles and are discussed as ideal information carriers in spintronics^{5–12}.

When a magnetic field is applied in the opposite direction to the magnetic moment of the skyrmion center, the Zeeman energy leads to a compression of the skyrmion^{13–15}. When the magnetic field reaches a critical value B_c , the core of the skyrmion will reverse its magnetization and align to the FM background. This mechanism is called the collapse of the skyrmion. In the continuum limit, the collapse of skyrmions occurs when their radii shrink down to zero¹⁶, while on a finite lattice of magnetic atoms, the radius reaches a finite value before the collapse^{14,16}. Skyrmion collapse with its abrupt change of the topology is associated with an energetic barrier and is usually studied as being thermally activated within the framework of transition state theory¹⁷.

Transition state theory requires the exploration of high energy states, the so-called saddle points, via the nudged elastic band (NEB)¹⁸. In magnetism, NEB has been extended to take into account the constant size of the magnetic moments and is known as the geodesic nudged elastic band (GNEB)^{19,20}. This method has been used

extensively to study the thermally activated probability of skyrmion collapse in strong ferromagnets such as Co/Pt(111)¹⁴ and in ultrathin magnetic films such as Pd/Fe/Ir(111)^{21–23}. Recently, more approaches for thermally activated skyrmion collapse have been proposed via Langevin magnetization dynamics simulation²⁴.

Although the thermally activated transition of single skyrmions to a ferromagnetic state has been extensively studied, the exploration of the transition by ramping up the external magnetic field at low temperatures — which involves the exploration of the saddle point — remains unexplored. This low temperature transition is particularly important in spin-polarized STM experiments which are done at cryogenic temperatures on ultra-thin films^{25,26}. In Pd/Fe/Ir(111) the transition between the skyrmion lattice phase and the FM phase as a function of the external magnetic field has been measured at 4 K^{13,25}. The skyrmion radius decreases as the magnetic field increases. However, in Pd/Fe/Ir(111), the large value of B_c did not allow the exploration of the saddle point¹³.

Compared to the experiment, the saddle point configuration is easy to explore in calculations since the magnetic configuration can be constrained. At this point, the magnetic moments are expected to align in-plane to create a vortex whose size is only several unit cells²⁰. This vortex unwinds the skyrmion and cancels the topological stabilization. Recently, the saddle point configurations were explored theoretically and it was found that even when the magnetic interactions are described in the continuum limit, a skyrmion of finite size could be expected as the saddle point configuration²⁷.

Here, we study the skyrmion collapse field B_c of isolated skyrmions in Co islands of single atomic thickness

on Ru(0001). In a previous work²⁶, we have combined spin-polarized STM measurements and DFT calculations to explore the ground state properties of Co/Ru(0001) and showed that skyrmions were stabilized by a vanishing effective anisotropy in combination with a small DMI. This particular ratio of magnetic interactions makes Co/Ru(0001) a prototypical soft ferromagnet in which isolated skyrmions have been stabilized at down to zero external magnetic fields. We experimentally determine B_c for skyrmion annihilation at minimal thermal activation using a dilution refrigerated STM with $T \approx 30$ mK²⁸. We numerically estimate B_c based on ab-initio parameters and find that it agrees well with experimental observations.

The ground state of Co/Ru(0001) in zero external magnetic field is a spin spiral of unique rotational sense and a periodicity of 37 nm²⁶. When a magnetic field B is applied normal to the surface, the spin spiral successively transforms into isolated skyrmions with radii depending on the external magnetic field. In our previous work, the spin structures were studied using tunneling anisotropic magneto-resistance (TAMR) and tunneling magneto-resistance (TMR). Here, we exclusively used the TAMR signal to determine the shape of the skyrmions to avoid magnetic dipole interactions between the tip and the sample and tracked the skyrmion dimensions as a function of magnetic field as shown Fig. 1. Note that in these maps of the differential conductivity dI/dV recorded at -350 mV, areas of an in-plane magnetization appear bright (higher dI/dV) opposed to areas with an out-of-plane magnetization appearing black (lower dI/dV)^{26,29,30}. Although the Ru substrate becomes superconducting below a critical temperature of ≈ 500 mK, all measurements presented were obtained in magnetic fields above the superconducting upper critical field of ≈ 5 mT, i.e. in the normal state of the substrate³¹. In our experiments, skyrmions were formed first applying 250 mT. Then, the B was reduced to the remanence of the superconducting magnet (≈ 7 mT) and metastable skyrmions remained. After this formation step, B was increased again to the indicated magnitudes to study the evolution of the skyrmion dimensions as function of B .

For fields below $B_c = 230$ mT, the skyrmions are found to be not round but elongated as seen in the left inset of Fig. 1. This is due to their tendency to reform the spin-spiral state at low fields via an instability against elongation. Thus, we determined the largest and smallest axis of the elongated skyrmion indicated in orange and green lines in the left inset and open circles in the figure. At fields higher than 230 mT, the skyrmions are round objects (see right inset of Fig. 1). The dI/dV signal varies as $\cos^2(\theta)$, with θ the azimuthal angle. The function used to fit the radius of the skyrmion is then³²:

$$dI/dV = \begin{cases} \cos^2\left(\frac{\pi \rho}{\sigma}\right) & \text{if } \rho \leq \sigma \\ 0 & \text{otherwise} \end{cases}, \quad (1)$$

where ρ is the distance from the center of the skyrmion, and σ is the radius of the skyrmion. The distance from

Figure 1. Theoretical (blue filled circles) values of $\sigma/2$ of the skyrmion versus applied magnetic field in Co/Ru(0001) together with the experimental values for round skyrmions $B > B_c \approx 230$ mT as illustrated in the right inset. At $B < B_c$, the skyrmions are elongated and both the radii along the long (orange) and short (green) axis are plotted as illustrated in the left inset. The black dashed curve is a fit to a/B . At fields in the shaded green area, annihilation of skyrmions was experimentally observed. The insets are differential conductance maps (white level proportional to dI/dV)

of 130x130 nm, $V = -350$ mV, $I = 2$ nA, modulation: $U = 60$ mV. left inset: $B = 0$ mT, right inset: $B = 400$ mT.

the center of the skyrmion to the maximum brightness in the dI/dV maps thus corresponds to half the skyrmion radius. We fitted the dI/dV contrast as shown in the right inset of Fig. 1 via eq. (1) to obtain the skyrmion radii for different magnetic fields. The radii of the round skyrmions as a function of the magnetic field are shown as red dots in Fig. 1. At lower fields, the scatter in the data is explained by the mentioned elliptical instability and the skyrmions' sensitivity to the near spin-spiral phase. As the field increases, these effects become marginal and the radius of the different skyrmions converges to the same value.

At higher field, analytical models predict the radius of isolated skyrmions to scale as $1/B^{33,34}$ as indicated by a fit to the high field experimental data (black dashed line). At fields below B_c , this relation necessarily breaks down, as the ground state is not a single, infinitely extended skyrmion³⁵ but the spin-spiral phase. Note that for the elongated skyrmions, the short axis half radius saturates around 12 nm corresponding to a local periodicity of the spin-spiral of ≈ 48 nm, i.e. at similar dimensions as the periodicity of the spin spiral²⁶. The long axis expands further in order to transform into the spin-spiral phase. Due to the neighboring spin spirals in the sample and the finite sample size, the long axis, however, does not diverge to infinity. In other words a kinetic barrier to go back to the spin-spiral phase allows for metastable skyrmions at vanishing fields. At fields larger than B_c the round skyrmions are compressed and the radii keep decreasing but stay finite until $B = 700$ mT. At this field, the collapse region is reached and individual skyrmions disappear by annihilating the topological charge (and do not reappear upon lowering the field again). When the field reaches $B = 800$ mT all skyrmions have disappeared which shows that the collapse field B_c was reached at $B_c = 750 \pm 50$ mT. As all measurements are made at $T \approx 30$ mK, this collapse is not due to thermal activation. Moreover, during ramping the field, the tip was retracted such that an influence of the tunneling current on the skyrmion collapse was excluded.

The experimental measurements were compared with atomistic simulations utilizing the Spirit code³⁶ which describes the energy of the magnetic texture as:

Figure 2. Energy density distribution with respect to the FM state at $B = 750$ mT. (a) and (b): The skyrmion was relaxed with an easy axis in-plane anisotropy of $13 \mu\text{eV}$ and without DDI: (a) MAE contribution and (b) DDI contribution. (c) skyrmion relaxed with both DDI and an easy axis anisotropy out-of-plane of $60 \mu\text{eV}$. (d), (e) and (f): radial energy density distribution showing the MAE (d), the DDI (e) and both contribution (f). The integral of (a) and (c) are of comparable magnitude with 13.8 meV and 11.8 meV, respectively.

$$\begin{aligned}
 E = & - \sum_{ij} J_{ij} \mathbf{M}_i \mathbf{M}_j - \sum_{ij} \mathbf{D}_{ij} (\mathbf{M}_i \times \mathbf{M}_j) \\
 & - \sum_i M_s \mathbf{M}_i \mathbf{B} - \sum_i \kappa \mathbf{M}_{i,z}^2 \\
 & - \sum_{ij} \frac{\mu_0 M_s^2}{4\pi} \frac{\mathbf{M}_i \mathbf{M}_j r_{ij}^2 - (\mathbf{M}_i \mathbf{r}_{ij}) (\mathbf{M}_j \mathbf{r}_{ij})}{r_{ij}^5}, \quad (2)
 \end{aligned}$$

where J_{ij} is the magnetic exchange interaction, \mathbf{D}_{ij} is the Dzyaloshinskii-Moriya vector, κ is the magnetocrystalline anisotropy (MAE) and \mathbf{B} is the external magnetic field. The magnetic interaction parameters, obtained by DFT in a previous publication²⁶, are $J_1 = 13.1$ meV, $D_1 = 0.2$ meV, $\kappa = -0.013$ meV and $M_s = 1.8 \mu_B$. Using these parameters, the experimental setup was modelled by a periodic superlattice containing 1000×1000 magnetic moments on a hexagonal lattice with the Ru lattice parameter of $a = 0.27$ nm. For each magnetic field H an isolated skyrmion was relaxed to its minimum of energy at which the skyrmion radius was fitted with eq. (1).

As in Ref.[30], the radius of the skyrmion without the dipole-dipole interaction (DDI) was calculated as a function of the field (blue dots in Fig. 1). Compared to the experiment, the radius decreases more steeply with increasing field but follows the same trend and matches well at higher fields. This discrepancy at lower fields is to be expected as the experimental skyrmions are more densely packed which leads to additional skyrmion compression compared to the simulations. The atomistic simulations predict a collapse field of $B_c = 820 \pm 10$ mT which is in good agreement with the experimental value. Considering that all theoretical parameters were obtained from DFT, the agreement between the atomistic simulations and the experiments is extremely good. This is particularly remarkable as tiny modifications of the anisotropy on the scale of the DFT-accuracy result in drastic modifications of the skyrmion radii and B_c in this fragile regime of atomistic parameters.

Additionally including the often neglected DDI demonstrates the delicate balance of atomistic parameters in this soft magnet. First, the DDI was evaluated in a magnetic configuration that was minimized neglecting it (Fig. 2 a,b,d,e). The energy gain of the skyrmion compared to the ferromagnetic state through the DDI is more than 5 times the gain of the MAE. Nevertheless, qualitatively both distributions do not differ much except for

Figure 3. GNEB calculation for $B = 0.55$ mT (blue) and $B = 0.75$ mT (orange) with zoom-in between 485 and 545 meV. The right inset shows the magnetic field dependence of the GNEB energy barrier. The four left insets depict the distributions of the z-component of the magnetization including zooms of the saddle-point core.

the non-vanishing energy gain at the core in case of the DDI. This is consistent with the common 2D interpretation of the DDI as shape anisotropy which can be absorbed into an effective magnetic anisotropy³⁷. Due to the relatively large magnitude of the DDI in this fragile system, the magnetic ground state changes drastically when the DDI is included. The background magnetization tilts in-plane in the experimentally investigated field range and skyrmions in an out-of-plane background are only viable in a small region around 1.5 T. In order to regain the previous agreement with experiment, the MAE as smallest parameter with large theoretical uncertainty and similar impact was tuned to $\kappa = -0.06$ meV which approximately counters the energy gain through the DDI. While the shape of the energy gain from the effective anisotropy shifts towards the core when including the DDI and modifying κ (Fig. 2 c,f), the previous dependence of the skyrmion radius on the field is recovered (not shown). Hence, the experimental results can also be described when including DDI, although a reasonable but arbitrary modification to the MAE is necessary.

Since DDI is not required to study the stability of skyrmions in ultra-thin films, we have explored the energy barrier without explicitly considering DDI in the vicinity of B_c via GNEB simulations¹⁹ on a 400×400 grid as shown in Fig. 3. The simulations were initialized with the relaxed skyrmion profile for a given magnetic field. Along the reaction path, the skyrmion shrinks until it reaches the saddle point which corresponds to the maximum of energy. The energy maximizes as the half radius reaches about 2 nm after which the core reverses and the ferromagnetic state is quickly attained (towards the right side of the figure). In that respect, even at the saddle point, we confirm numerically that in soft ferromagnets a finite radius skyrmion solution exists as predicted in Ref.[27].

When the external magnetic field is increased, the energy barrier decreases drastically (right inset of Fig. 3) reaching 0.5 meV at 800 mT. For all the magnetic fields, the skyrmion solution at the saddle point has a finite radius. The initial flat section of the energy evolution easily allows variation of the skyrmion radius in the vicinity of B_c while the very small barrier at B_c prohibits direct observation of the skyrmion collapse. Still, with the minimal experimental skyrmion half radius of ≈ 3.1 nm the direct vicinity of the collapse is observed to a good approximation and all further compression leads to vanishing of the barrier (or tunneling) on timescales too small for observation.

To conclude, the collapse path of a skyrmion was stud-

ied in the prototypical soft ferromagnet Co/Ru(0001). As expected, the radius of the skyrmion decreases monotonically as the magnetic field increases up to the collapse field B_c . We have reproduced the experimental skyrmion radii and computed B_c based on atomistic simulation parameterized by DFT calculation. Both experimental and computational method confirm that its radius does not reach zero even at the saddle point and that the DDI can be correctly approximated by an effective anisotropy in 2D ultra-thin films.

The data that support the findings of this study are available from the corresponding author upon reasonable request.

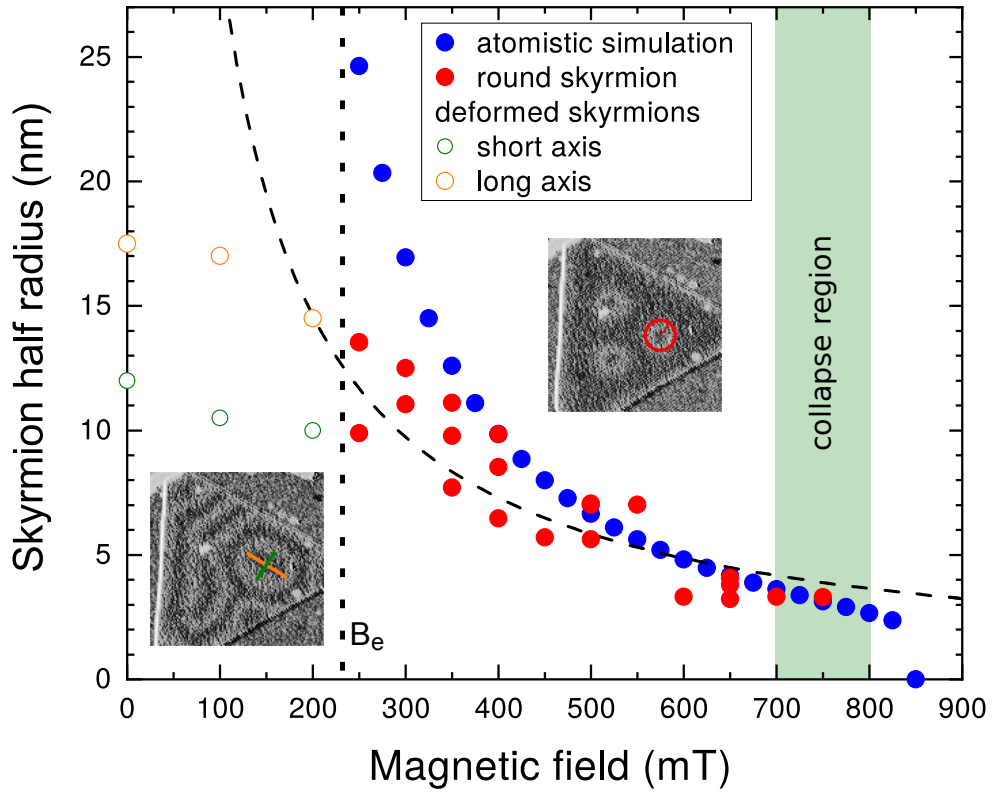
B. Dupé and P. Buhl acknowledge useful discussion with J.V. Kim and U. Ritzmann. W. Wulfhekel and L. Mougél acknowledge funding by the Deutsche Forschungsgemeinschaft (DFG) under the grant WU 349/15-1 and WU 349/16-1. B. Dupé and P. Buhl acknowledge funding by the DFG under the grant DU 1489/3-1.

REFERENCES

- ¹A. N. Bogdanov and A. Hubert, *Phys. stat. solid.* **186**, 527 (1994).
- ²U. K. Rössler, A. N. Bogdanov, and C. Pfleiderer, *Nature* **442**, 797 (2006).
- ³A. N. Bogdanov and D. Yablonskii, *Zh. Eksp. Teor. Fiz.* **95**, 178 (1989).
- ⁴A. Fert and P. M. Levy, *Phys. Rev. Lett.* **44**, 1538 (1980).
- ⁵N. S. Kiselev, A. N. Bogdanov, R. Schäfer, and U. K. R. Ler, *Journ. Phys. D* **44**, 392001 (2011).
- ⁶F. Jonietz, S. Mühlbauer, C. Pfleiderer, A. Neubauer, W. Münzer, A. Bauer, T. Adams, R. Georgii, P. Böni, R. A. Duine, K. Everschor, M. Garst, and A. Rosch, *Science* **330**, 1648 (2010).
- ⁷A. Fert, V. Cros, and J. Sampaio, *Nature Nano.* **8**, 152 (2013).
- ⁸J. Sampaio, V. Cros, S. Rohart, A. Thiaville, and A. Fert, *Nature Nano.* **8**, 839 (2013).
- ⁹N. Nagaosa and Y. Tokura, *Nature Nano.* **8**, 889 (2013).
- ¹⁰A. Fert, N. Reyren, and V. Cros, *Nature Reviews Materials* **2**, 17031 (2017).
- ¹¹T. Nozaki, Y. Jibiki, M. Goto, E. Tamura, T. Nozaki, H. Kubota, A. Fukushima, S. Yuasa, and Y. Suzuki, *Appl. Phys. Lett.* **114**, 012402 (2019).
- ¹²C. Ma, X. Zhang, J. Xia, M. Ezawa, W. Jiang, T. Ono, S. N. Piramanayagam, A. Morisako, Y. Zhou, and X. Liu, *Nanolett.* **19**, 353 (2019).
- ¹³N. Romming, A. Kubetzka, C. Hanneken, K. von Bergmann, and R. Wiesendanger, *Phys. Rev. Lett.* **114**, 177203 (2015).
- ¹⁴S. Rohart, J. Miltat, and A. Thiaville, *Phys. Rev. B* **93**, 214412 (2016).
- ¹⁵A. Bernard-Mantel, L. Camosi, A. Wartelle, N. Rougemaille, M. Darques, and L. Ranno, *SciPost Phys.* **4**, 027 (2018).
- ¹⁶A. Leonov, T. L. Monchesky, N. Romming, A. Kubetzka, A. N. Bogdanov, and R. Wiesendanger, *New J. Phys.* **18**, 065003 (2016).
- ¹⁷E. Wigner, *Trans. Faraday Soc.* **34**, 29 (1938).
- ¹⁸G. Henkelman, B. P. Uberuaga, and H. Jónsson, *J. Chem. Phys.* **113**, 9901 (2000).
- ¹⁹P. F. Bessarab, V. M. Uzdin, and H. Jónsson, *Phys. Rev. B* **85**, 184409 (2012).
- ²⁰P. F. Bessarab, V. M. Uzdin, and H. Jónsson, *Computer Physics Communications* **196**, 335 (2015).
- ²¹S. von Malottki, B. Dupé, P. F. Bessarab, A. Delin, and S. Heinze, *Scientific Reports* **7**, 12299 (2017).
- ²²P. F. Bessarab, G. P. Müller, I. S. Lobanov, F. N. Rybakov, N. S. Kiselev, H. Jónsson, V. M. Uzdin, S. Blügel, L. Bergqvist, and A. Delin, *Sci. Rep.* **8**, 3433 (2018).
- ²³S. von Malottki, P. F. Bessarab, S. Haldar, A. Delin, and S. Heinze, *Phys. Rev. B* **99**, 060409 (2019).
- ²⁴L. Desplat, C. Vogler, J.-V. Kim, R. L. Stamps, and D. Suess, *Phys. Rev. B* **101**, 060403 (2020).
- ²⁵N. Romming, C. Hanneken, M. Menzel, J. E. Bickel, B. Wolter, K. von Bergmann, A. Kubetzka, and R. Wiesendanger, *Science* **341**, 636 (2013).
- ²⁶M. Hervé, B. Dupé, R. Lopes, M. Böttcher, M. D. Martins, T. Balashov, L. Gerhard, J. Sinova, and W. Wulfhekel, *Nat. Commun.* **9**, 1015 (2018).
- ²⁷B. Heil, A. Rosch, and J. Masell, *Phys. Rev. B* **100**, 134424 (2019).
- ²⁸T. Balashov, M. Meyer, and W. Wulfhekel, *Rev. Sci. Instrum.* **89**, 113707 (2018).
- ²⁹M. Bode, S. Heinze, A. Kubetzka, O. Pietzsch, X. Nie, G. Bihlmayer, S. Blügel, and R. Wiesendanger, *Phys. Rev. Lett.* **89**, 237205 (2002).
- ³⁰M. Hervé, T. Balashov, A. Ernst, and W. Wulfhekel, *Phys. Rev. B* **97**, 220406 (2018).
- ³¹D. K. Finnemore and D. E. Mapother, *Phys. Rev. Lett.* **9**, 288 (1962).
- ³²K. von Bergmann, M. Menzel, D. Serrate, Y. Yoshida, S. Schröder, P. Ferriani, A. Kubetzka, R. Wiesendanger, and S. Heinze, *Phys. Rev. B* **86**, 134422 (2012).
- ³³A. N. Bogdanov and A. Hubert, *J. Magn. Magn. Mater.* **138**, 255 (1994).
- ³⁴M. N. Wilson, A. B. Butenko, A. N. Bogdanov, and T. L. Monchesky, *Phys. Rev. B* **89**, 094411 (2014).
- ³⁵A. N. Bogdanov and A. Hubert, *J. Magn. Magn. Mater.* **195**, 182 (1999).
- ³⁶G. P. Müller, M. Hoffmann, C. Dißelkamp, D. Schürhoff, S. Mavros, M. Sallermann, N. S. Kiselev, H. Jónsson, and S. Blügel, *Phys. Rev. B* **99**, 224414 (2019).
- ³⁷E. Feldtkeller and H. Thomas, *Physik der Kondensierten Materie* **4**, 8 (1965).

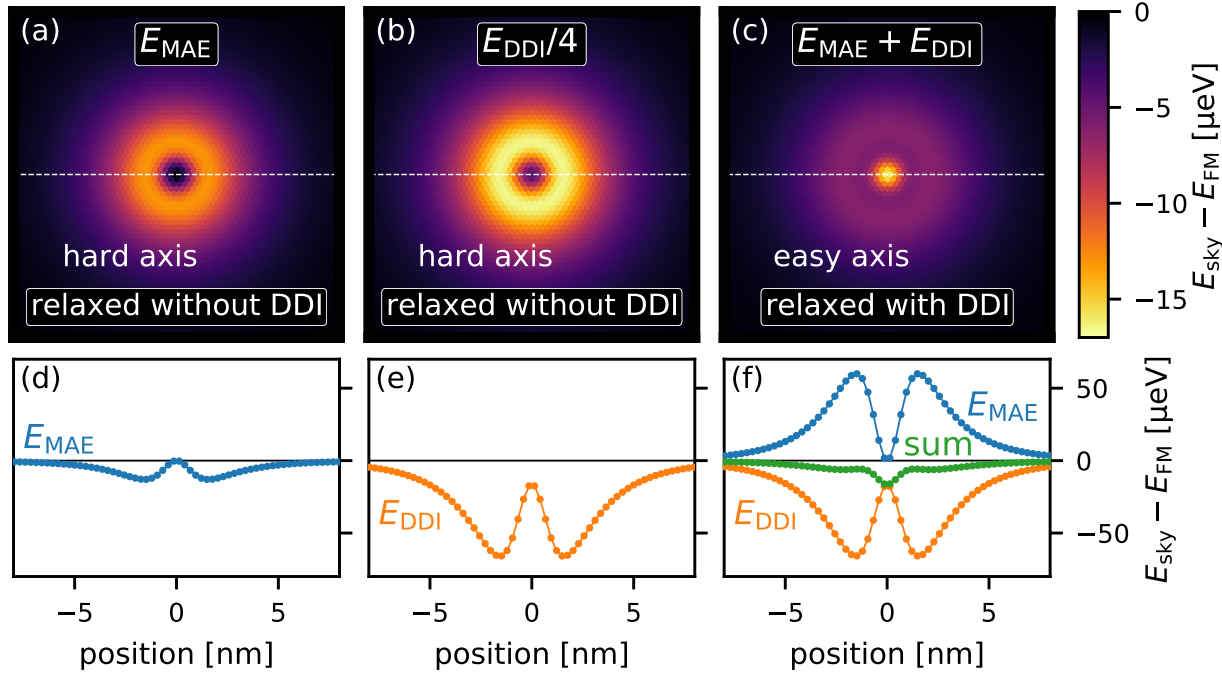
This is the author's peer reviewed, accepted manuscript. However, the online version of record will be different from this version once it has been copyedited and typeset.

PLEASE CITE THIS ARTICLE AS DOI: 10.1063/5.0013488



This is the author's peer reviewed, accepted manuscript. However, the online version of record will be different from this version once it has been copyedited and typeset.

PLEASE CITE THIS ARTICLE AS DOI: 10.1063/5.0013488



This is the author's peer reviewed, accepted manuscript. However, the online version of record will be different from this version once it has been copyedited and typeset.

PLEASE CITE THIS ARTICLE AS DOI: 10.1063/5.0013488

